ACS Partner Journal

CHEMICAL & BIOMEDICAL IMAGING

pubs.acs.org/ChemBioImaging

Article

Single-Molecule Spectroscopy Reveals the Plasmon-Assisted Nanozyme Catalysis on AuNR@TiO_2

Li Zuo, Hallie King, Mohammad Akter Hossain, Fatiha Farhana, Madelyn M. Kist, Rebecca L. Stratton, Jiao Chen, and Hao Shen*

Cite This: *Chem. Biomed. Imaging* 2023, 1, 760–766

Read Online

ACCESS | Metrics & More | Article Recommendations | Supporting Information

ABSTRACT: Gold nanoparticles are frequently employed as nanozyme materials due to their capacity to catalyze various enzymatic reactions. Given their plasmonic nature, gold nanoparticles have also found extensive utility in chemical and photochemical catalysis owing to their ability to generate excitons upon exposure to light. However, their potential for plasmon-assisted catalytic enhancement as nanozymes has remained largely unexplored due to the inherent challenge of rapid charge recombination. In this study, we have developed a strategy involving the encapsulation of gold nanorods (AuNRs) within a titanium dioxide (TiO_2) shell to facilitate the efficient separation of hot electron/hole pairs, thereby enhancing nanozyme reactivity. Our investigations have revealed a remarkable 10-fold enhancement in reactivity when subjected to 530 nm light excitation following the introduction of a TiO_2 shell. Leveraging single-molecule kinetic analyses, we discovered that the presence of the TiO_2 shell not only amplifies catalytic reactivity by prolonging charge relaxation times but also engenders additional reactive sites within the nanozyme's intricate structure. We anticipate that further enhancements in nanozyme performance can be achieved by optimizing interfacial interactions between plasmonic metals and semiconductors.

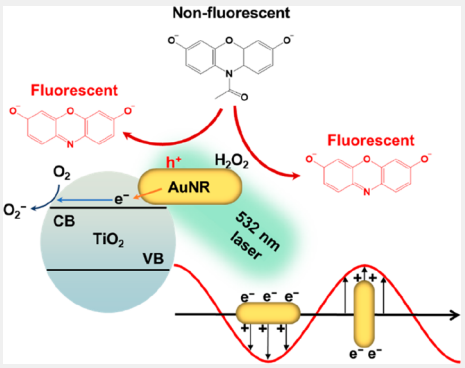

KEYWORDS: *single-molecule, nanozyme, plasmon-assisted catalysis, AuNR@TiO_2, reactivity enhancement*

1. INTRODUCTION

Recent investigations have led to the emergence of artificial enzymes, including nanozymes[1−5] and DNAzymes,[6,7] which have been strategically designed to address the inherent limitations of natural enzymes, particularly those pertaining to cost and stability. Notably, metal-based nanozymes,[8−16] including gold (Au), platinum (Pt), and copper (Cu), have gathered substantial attention across a variety of everyday applications such as biosensing,[10−12,17] cancer therapy,[9,13,14] and environmental pollutant remediation.[15] Gold (Au) has emerged as a particularly promising candidate among these metallic elements due to its remarkable biocompatibility and surprisingly broad natural enzyme-mimicking capabilities. These Au-based nanozymes consist of Au nanoparticles enveloped in polymers or biomolecules, thereby enhancing their biocompatibility, reactivity, and selectivity. Consequently, they have emerged as highly promising alternatives to their natural enzyme counterparts.

Being a plasmonic metal, Au has found extensive application in enhancing chemical and photochemical reactivities through its surface plasmon resonance (SPR). Regrettably, discussions concerning the integration of SPR into nanozyme designs remain relatively scarce. Pristine, uncoated gold nanoparticles manifest SPR when subjected to incident light, thereby generating hot charge carriers conducive to catalysis. The SPR phenomenon exhibits notable tunability due to its robust morphology-dependent characteristics. Consequently, nanocatalysts frequently harness the unique attributes of Au to enhance their performance, exemplified in applications like CO oxidation and water-splitting reactions.[18−22] Nonetheless, using SPR to enhance the efficacy of Au-based nanozymes remains relatively underexplored.[23−25] A primary hindrance in this regard is the rapid recombination of hot electrons and holes within the Au structure. This phenomenon significantly diminishes the practical utility of SPR-generated hot charges.[19,26,27] Therefore, it is crucial to functionalize the surface of Au-based nanozymes and meticulously optimize the coating geometry to mitigate the charge recombination rate. Since their wide bandgap characteristics optimize charge separation efficiency, semiconductor materials are highly suitable candidates for Au modifications. Through the grafting of semiconductors onto Au, SPR-generated hot electrons undergo injection into the conduction band of the semi-

Received: September 10, 2023
Revised: October 16, 2023
Accepted: October 25, 2023
Published: November 10, 2023

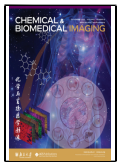

https://doi.org/10.1021/cbmi.3c00096
Chem. Biomed. Imaging 2023, 1, 760−766

conductors via Schottky junctions, thereby facilitating reduction reactions at the semiconductor interface. Concurrently, the remaining holes on the Au surface serve as reactive sites for oxidation reactions.[26,28−30]

Au−semiconductor hybrid nanozymes can be synthesized by growing Au nanoparticles (AuNP) on specific semiconductor supports through various wet-chemistry methods.[9,31−34] However, this approach usually lacks precise morphological control of the resulting AuNP, thereby limiting the effectiveness of stimulating SPR. Alternatively, one could control the growth of semiconducting particles onto AuNP.[20,35,36] This method preserves the size and shape of the original AuNP, offering better control of the SPR. Notably, semiconducting coatings on AuNPs do not always lead to improved catalytic activity. In fact, they may block light absorption by AuNP or hinder mass transport during catalysis, resulting in an overall decrease in reactivity. Therefore, researchers might benefit from engineering porous structures or adjusting surface hydrophobicity to overcome the limitations of Au−semiconductor hybrid nanozymes.[36−40]

In this study, we synthesized a core−shell Au nanorod−TiO_2 nanozyme (AuNR@TiO_2) using a precipitation method and focused on investigating its peroxidase mimic properties in catalyzing the N-deacetylation oxidation of Amplex Red (AR). A remarkable 10-fold enhancement in reactivity was observed for the AuNR@TiO_2 nanozyme under 530 nm light excitation compared to the unmodified parent AuNRs. To address the inherent reactivity heterogeneity of individual nanozymes, we employed single-molecule microscopy to assess the catalytic reactivity of each nanozyme separately. Importantly, the resulting AuNR@TiO_2 remained plasmon-active, and the thin TiO_2 shell surrounding the AuNR core did not impede AR from accessing the AuNR surfaces. With an increase in excitation light power, both the SPR and laser-induced heating contributed to the enhanced reactivity of the AuNR@TiO_2 nanozymes. Upon analysis of the reactivity fluctuations during catalysis, we discovered that synergistic interactions between the plasmonic metal core (AuNR) and the semiconductor shell (TiO_2) generated additional reactive sites for catalysis.

2. EXPERIMENTAL SECTION

2.1. Synthesis of AuNR@TiO_2 Nanoparticles

The synthesis procedure is detailed in the Supporting Information. Briefly, titanium trichloride ($TiCl_3$) was used as the precursor. TiO_2 was formed through pH-mediated hydrolysis followed by H_2O_2-facilitated oxidation:[36]

$$Ti^{3+} + 2H_2O \rightarrow TiO_2 + 4H^+ + e^-$$

$$2H^+ + 2e^- \rightarrow H_2$$

The resulting particles were thoroughly rinsed and redispersed into DI-water.

2.2. Ensemble Catalysis

To assess the performance, we conducted ensemble activity measurements for AuNR and AuNR@TiO_2, separately, utilizing the oxidative N-deacetylation of AR as the catalytic reaction for both investigations. These reactions were conducted in a 50 mM pH 7.4 phosphate buffer by introducing the AuNR or AuNR@TiO_2 into a premixed reactant solution containing AR and 60 mM H_2O_2. The reaction product displays fluorescence activity, and its emission was recorded using an Agilent Cary60 fluorometer. To investigate the impact of SPR, we introduced an LED light source to illuminate the solution mixture during the reaction. As control experiments, we also conducted commercial TiO_2-catalyzed AR oxidation assays with and without the presence of LED illumination.

2.3. Single-Molecule Catalysis

Single-particle catalysis experiments utilized a total internal reflection (TIR) fluorescence microscope (based on an Olympus IX83). To create a microfluidic reaction chamber, approximately 20 μL of ∼5 pM colloidal AuNR or AuNR@TiO_2 solution was drop-cast onto a VWR #1 glass coverslip measuring 25 × 25 mm^2. After a 3 min rinsing with DI-water to eliminate unbound nanozymes, this coverslip was integrated into a 25 mm (length) × 10 mm (width) × 100 μm (height) microfluidic cell assembly, utilizing double-sided tape, a microscope slide (Thermo Scientific), and epoxy glue. Two holes were drilled into the microscope slide to accommodate polyethylene tubing connections, facilitating the continuous supply of the premixed reactant solution (0.05−1.8 μM AR, 60 mM H_2O_2, and 50 mM pH 7.4 phosphate buffer) via a syringe pump (Genie Touch, Kent Scientific) at a rate of 20 μL/min during the measurement.

For the excitation of fluorescence emission, a 532 nm continuous-wave laser beam (DragonLaser) was focused onto an area of 35 × 35 μm^2 within the microfluidic cell. The laser power was adjusted within the 3 mW/cm^2 range to 35 mW/cm^2 by using a graduated neutral density filter. Emission signals were collected using a 100× NA 1.49 oil immersion objective (UAPON 100xOTIRF, Olympus), filtered through a long-pass filter (Chroma, ET542lp) and a bandpass filter (Chroma ET575/50m). The resulting signals were captured using an sCMOS camera (Photometrics Prime 95B) through the Olympus CellSens Dimension software at a frame rate of 50 ms. Subsequently, the fluorescence signals were analyzed using ThunderSTORM,[41,42] in conjunction with our custom-written Matlab programs. Detailed procedures for data processing are shown in the Supporting Information.[43]

3. RESULTS AND DISCUSSION

AuNR@TiO_2 nanoparticles were synthesized by using $TiCl_3$ as the precursor. We achieved the desired core−shell morphology (AuNR@TiO_2) by meticulously controlling the hydrolysis of $TiCl_3$ (Supporting Information, Section 1). Transmission electron microscopy (TEM) images revealed a thin uniformly distributed TiO_2 layer surrounding the AuNR (Figure 1a and b). The presence of TiO_2 was further confirmed via energy-dispersive X-ray spectroscopy (EDX), as depicted in Figure S2. UV−vis spectra were recorded to examine the optical properties of AuNRs@TiO_2 (Figure 1c). The original 18 × 54 nm^2 AuNRs exhibited longitudinal and transverse surface plasmon resonances at 685 and 517 nm, respectively. Notably, both SPR peaks displayed clear redshifts following TiO_2 deposition. Specifically, the longitudinal plasmon band shifted to 715 nm, accompanied by a significant decrease in absorbance. This phenomenon aligns with previous findings[44−46] and is attributed to the alteration in the local refractive index surrounding the AuNR after the TiO_2 coating process. In addition, the curvature in the tip of AuNR increased the alteration in the local refractive index, causing further inhibition to longitudinal SPR.[36]

Au-based materials have proven to be highly valuable as peroxidase mimics, finding extensive applications in various oxidative reactions.[10,31,47−50] In this study, we employed a well-established fluorogenic probe,[51,52] AR, to evaluate the catalytic properties of both AuNR and AuNR@TiO_2. As depicted in Figure 1d, the initially nonfluorescent AR underwent conversion into the highly fluorescent molecule resorufin (RF) in the presence of nanozymes and H_2O_2. We quantified the reaction rates by collecting fluorescence spectra at approximately 15 min intervals. Interestingly, we observed that the presence of the TiO_2 layer outside the AuNR did not

https://doi.org/10.1021/cbmi.3c00096
Chem. Biomed. Imaging 2023, 1, 760−766

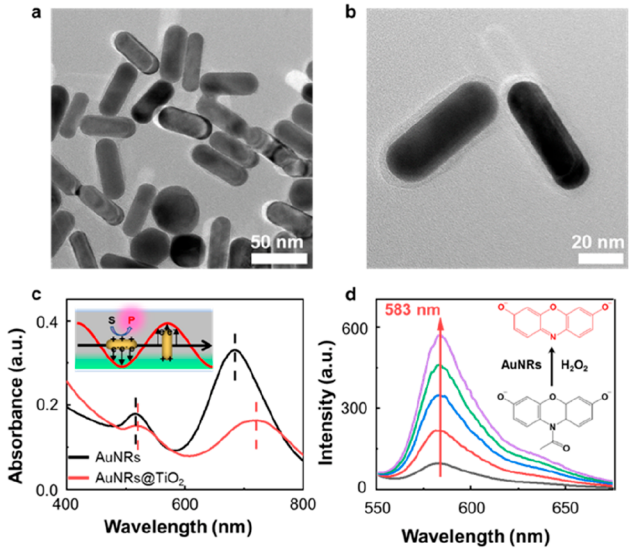

Figure 1. (a, b) TEM images of the AuNR@TiO_2 nanozymes. (c) UV−vis spectra of AuNRs and AuNRs@TiO_2. Inset: scheme of the plasmon-assisted chemical reaction on AuNR-based nanozymes. (d) AR oxidation measured by a fluorometer. The increasing intensity at ∼583 nm reflects the formation of fluorescent product RF. Inset: illustration of AR oxidation catalyzed by AuNR in the presence of H_2O_2.

significantly influence catalytic performance, as the AuNR@TiO_2 exhibited nearly identical reactivity to the bare AuNR (Figure S4a). Even under 700 nm LED illumination, there was only a slight increase in catalytic reactivity (Figure 2a), a

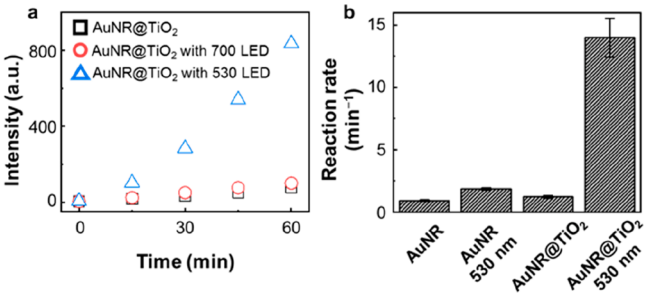

Figure 2. (a) Time-evolving fluorescence trajectories for AuNR@TiO_2 under 530 and 700 nm LED illumination. (b) AR oxidation rates on AuNR and AuNR@TiO_2, with and without a 530 nm LED illumination, calculated from the fitting of the time-evolving fluorescence intensity trajectories.

phenomenon that we attribute to the pronounced suppression of the longitudinal plasmon band after TiO_2 deposition. However, when subjected to 530 nm LED illumination at an intensity of approximately 12 mW/cm^2, a remarkable 10-fold enhancement in reactivity was observed (Figure 2b). The 530 nm LED light generates transverse SPR, directing hot electrons into the TiO_2 while retaining hot holes within the AuNR. This substantial reactivity enhancement is likely attributable to the formation of hot holes, as the reaction under investigation necessitates the involvement of two holes for completion. In comparison, the bare AuNR exhibited only a 2-fold reactivity enhancement (Figure 2b), which is likely due to rapid charge recombination, with mostly hot holes dissipating before converting AR into RF. These experiments clearly demonstrate AuNR@TiO_2 to be a plasmon-assisted nanozyme. The TiO_2 layer did not impede transverse plasmon formation but prolonged the relaxation time, resulting in distinct light-dependent reactivity.

To gain deeper insights into the reaction kinetics and overcome the limitation of ensemble averaging, we conducted single-molecule catalysis experiments for individual AuNRs and AuNR@TiO_2 nanozymes. These nanozymes catalyzed the same AR → RF reaction under steady-state conditions. It was found that each nanozyme catalyzed substrate conversion successively without mechanistic overlap. Upon generation, the product RFs swiftly detached from the nanozyme surface and were carried away by the flow created by the attached syringe pump. Consequently, the catalytic turnovers manifested as intermittent blinking fluorescence spots across the 35 × 35 μm^2 field of view. Each blinking event signified the formation of a single RF molecule (Figure 3a and b), and the time

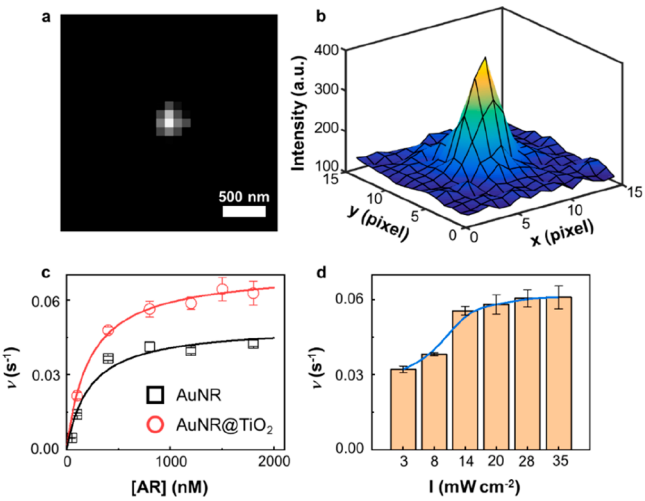

Figure 3. (a) A typical fluorescence image of a single RF molecule. Background emissions were removed. (b) Localizing an RF molecule in (a) by fitting its emission signal to a two-dimensional Gaussian function. The localization error is 5.2 nm. (c) Dependence of the single-particle turnover rate on AR concentration. The laser power was kept at 13 mW/cm^2. (d) Dependence of the turnover rate on the power of the 532 nm laser's power. The concentration of AR was kept at 800 nM. All experiments were performed at 60 mM H_2O_2. The error bars in (c) and (d) depict the standard error of the mean, and each data point represents an average of more than 60 nanozymes.

interval between two consecutive blinking events denoted the waiting time τ for RF formation. The inverse of the average τ, denoted as $\langle\tau\rangle^{-1}$, provided the turnover rates at the single-molecule level.[53,54]

It was revealed that both AuNR and AuNR@TiO_2 nanozymes displayed an increase in reactivity as the AR concentration increased until reaching their maximum reactivity and remaining constant (Figure 3c). This behavior can be effectively explained by a modified Michaelis−Menten mechanism[53,55]

$$\langle\tau\rangle^{-1} = k_{cat} n[S]/(K_M + [S]) \quad (1)$$

in which k_{cat} is the rate constant for a single reactive site, n is the number of reactive sites within one nanozyme, K_M is the Michaelis−Menten constant, and $[S]$ is the AR concentration. Fitting the titration curve with eq 1 provides the values of $k_{cat}n$ and K_M for AuNR and AuNR@TiO_2 nanozymes, as summarized in Table 1.

https://doi.org/10.1021/cbmi.3c00096
Chem. Biomed. Imaging 2023, 1, 760−766

Table 1. Catalytic Parameters

	$k_{cat}n$ (s^{-1})	K_M (μM)	$k_{cat}n/K_M$ ($s^{-1}\ \mu M^{-1}$)
AuNR	0.050 ± 0.004	0.22 ± 0.07	0.23 ± 0.04
AuNR@TiO_2	0.072 ± 0.002	0.20 ± 0.02	0.33 ± 0.02

Consistent with the results from ensemble measurements, it is noteworthy that the maximum reactivity of AuNR@TiO_2 surpassed its parent counterpart, AuNR. The catalytic rate constant ($k_{cat}n$) for AuNR@TiO_2 was 0.072 ± 0.002 s^{-1}, representing a 40% increase compared to that of AuNR, which exhibited a $k_{cat}n$ of 0.050 ± 0.004 s^{-1}. This difference indicates that either the per site reactivity has increased for AuNR@TiO_2 or the deposition of TiO_2 has introduced additional reactive sites in the nanozyme. However, the Michaelis–Menten constant (K_M) was found to be 0.22 ± 0.07 μM for AuNR@TiO_2, approximately the same as the AuNR which had a K_M of 0.20 ± 0.02 μM. This slight difference in K_M values suggests that the binding affinity of AR with AuNR@TiO_2 is comparable to that of pristine AuNR. Previous studies[36,38,56,57] have suggested that core–shell structures tend to cover the reactive sites on Au nanozymes, potentially inhibiting substrate adsorption onto the Au surface. However, this phenomenon did not manifest in our work, likely due to the mild hydrolysis of $TiCl_3$ and the subsequent formation of a porous TiO_2 shell. Additionally, the estimated average thickness of the TiO_2 shell was ~3 nm (Figure S3d), a dimension insufficient to impede mass transport significantly. Therefore, it is probable that the AR substrates can effectively interact with the AuNR surface after the TiO_2 deposition. A previous study indicates that the thickness of the TiO_2 shell could influence the overall reactivity of the catalyst by potentially altering the interaction between the substrate and the catalyst surface.[58] The catalytic efficiency ($k_{cat}n/K_M$) of AuNR@TiO_2 was calculated to be 0.33 ± 0.02 $s^{-1}\ \mu M^{-1}$, surpassing that of AuNR at 0.23 ± 0.04 $s^{-1}\ \mu M^{-1}$ by 43%. Furthermore, the reaction rates of individual AuNR and AuNR@TiO_2 displayed a broad distribution range, indicating substantial heterogeneity in reactivity among individual nanozymes (Figure 4a and b). The variance for single

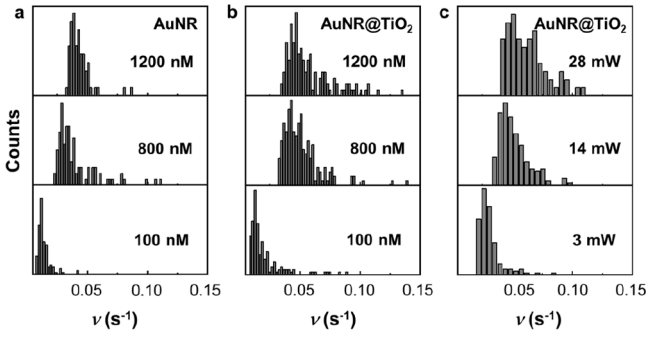

Figure 4. Distributions of the turnover rate for AuNR and AuNR@TiO_2. (a, b) AR concentration titration. (c) Laser-power-dependent reactivity for AuNR@TiO_2.

nanozyme turnover rate increased from 8.3 × 10^{-5} for AuNR at 1200 nM AR to 7.4 × 10^{-4} for AuNR@TiO_2 under the same condition. According to the previous study,[59] the escalation of variance is most likely due to the increase of reactive sites. This direct observation of reactivity heterogeneity is a unique feature offered by single-molecule measurements, which proves to be challenging to obtain through ensemble-averaged analyses.

It is noteworthy that the 532 nm laser used for fluorescence excitation also induces the transverse SPR of the AuNR, leading to the generation of electron–hole pairs (Figure 1c, inset). Since this laser is required for single-molecule detection, SPR enhancement contributed to the reactivity of both AuNR and AuNR@TiO_2 during the measurements. To systematically investigate the contributions from SPR, we incrementally increased the laser power at 532 nm from 3 to 35 mW/cm^2, while maintaining the AR concentration at 800 nM. We observed that the intensity dependence exhibited a modest superlinear trend (Figure 3d). Prior studies involving the complex of TiO_2 and AuNP have demonstrated that plasmon-induced catalysis depends linearly on the laser power. The superlinear behavior arises from the photothermal effect resulting from laser excitation.[60,61] Therefore, we conclude that both the SPR-induced hot electrons and holes and the photothermal effect collectively enhance the overall reactivity of the AuNR@TiO_2 nanozyme. Furthermore, in contrast to ensemble measurements with a low-power LED light, a laser-induced photothermal effect may boost the reactivity of both AuNR and AuNR@TiO_2 under such reaction conditions. Based on previous studies,[23,60,61] it is projected that the temperature in the vicinity of the AuNR may rise by approximately 1 K under the reaction conditions employed in our study (3–35 mW/cm^2). Therefore, we anticipate that the photothermal effect induced by the laser is a minor contributor to the observed enhancement in reactivity. The difference in reactivity between these two nanozymes also becomes less pronounced under such reaction conditions (Figure 3c and Table 1). However, increased excitation power appears to exacerbate the reactivity heterogeneity among nanozymes (Figure 4c), likely due to the creation of additional reactive sites.

As previously reported, the reactivity of a single nanozyme exhibits fluctuations over time (Figure 5a). In the case of metal nanoparticles such as Au and Pt, this fluctuation arises from surface restructuring during catalytic transformations, resulting in a "memory effect" within the waiting time τ sequence.[54,62] To unveil this memory effect, we calculated the autocorrelation function $C_\tau(m)$:

$$C_\tau(m) = \langle \Delta\tau(0)\Delta\tau(m)\rangle / \langle \Delta\tau^2\rangle$$

Here, m represents the index of a catalytic turnover for a single nanozyme and the lag is $\Delta\tau(m) = \tau(m) - \langle\tau\rangle$. We observed that the autocorrelation follows an exponential decay as the lag increases (Figure 5b), where the inverse of the correlation times provides the reactivity fluctuation rates (Figure 5c and d). Notably, the relationship between the fluctuation rate and the reaction rate is linear for bare AuNR (Figure 5c, black curve). This result can be attributed to the interplay of substrate–nanozyme interactions: higher substrate concentrations lead to accelerated reaction turnovers and faster surface restructuring.[53,54] Strikingly, the relationship becomes superlinear for AuNR@TiO_2, where a steeper slope is observed at high turnover rates. This suggests that the AuNR@TiO_2 nanozyme exhibits more pronounced fluctuations when the reaction turnover is rapid. Furthermore, it is worth noting that the reactivity fluctuation in AuNR@TiO_2 nanozymes does not necessarily stem from surface restructuring, as observed in bare AuNR. The introduction of additional reactive sites after the TiO_2 deposition would escalate the fluctuation rate, as well.

https://doi.org/10.1021/cbmi.3c00096
Chem. Biomed. Imaging 2023, 1, 760–766

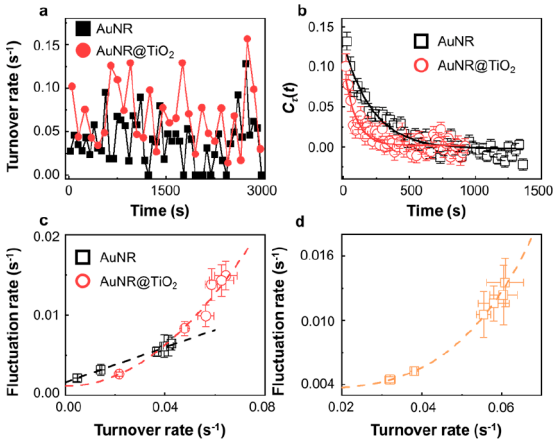

Figure 5. (a) The time-dependent turnover rate for a single AuNR and AuNR@TiO_2 nanozyme in catalyzing the AR oxidation. [AR] = 800 nM and [H_2O_2] = 60 mM. Turnover rates are calculated every 100 s. (b) Autocorrelation function $C_\tau(t)$ of the microscopic reaction time τ from the time sequence of AuNR (black square) and AuNR@TiO_2 (red circle) catalysis. Each curve is an average of more than 60 nanozymes. The solid lines are fits with single exponential decay functions. The decay time constants are 220 ± 17 s (AuNR) and 89 ± 13 s (AuNR@TiO_2), respectively. (c, d) Dependence of fluctuation rates on [AR] (c) and laser power (d). The *y*-axis is the inverse of the reactivity fluctuation correlation time obtained from $C_\tau(t)$. The superlinear curves are fits using $y = y_0 + kx^\gamma$, where γ is the photothermal factor.

Moreover, the photothermal effect also contributed to the reactivity fluctuation. Thus, an empirical superlinear function $y = y_0 + kx^\gamma$ was used to fit the reactivity fluctuation trend. The photothermal factor γ was determined to be 1.54 ± 0.11. We further investigated the laser-power-dependent fluctuation rates for AuNR@TiO_2 nanozymes (Figure 5d). The dependence of fluctuation rates does not follow a linear trend, further supporting the formation of additional reactive sites due to hot electron injection into the conduction band of TiO_2 via the Schottky junction. The photothermal factor γ was increased to 1.64 ± 0.12, as a result of varying the laser power.

4. CONCLUSION

In conclusion, we successfully synthesized a core−shell AuNR@TiO_2 nanozyme capable of harnessing SPR to significantly enhance the catalytic reactivity. Our systematic investigation included both ensemble and single-molecule analyses. Remarkably, a thin and porous TiO_2 shell on a AuNR led to an impressive ∼43% increase in catalytic efficiency rather than passivating the nanoparticle surface as expected. The induction of SPR through light excitation resulted in a striking 10-fold enhancement in the reactivity of the AuNR@TiO_2 nanozyme, due to the generation of additional reactive sites following the injection of hot electrons and holes into the conduction band of TiO_2. The heightened reactivity, increased variance in the single turnover time, and intensified reactivity fluctuations collectively indicate the emergence of additional reactive sites following TiO_2 deposition. The well-orchestrated Au−TiO_2 interactions synergistically extend the charge recombination time, resulting in SPR-assisted catalysis. We anticipate that further improvements in the performance of this complex nanozyme can be achieved through optimization of each component's structure.

■ ASSOCIATED CONTENT

Supporting Information

The Supporting Information is available free of charge at https://pubs.acs.org/doi/10.1021/cbmi.3c00096.

Detailed procedure of the AuNR@TiO_2 nanozyme synthesis; TEM images and size distributions; UV−vis spectra; fluorogenic probing reaction; single-molecule data analysis; and catalytic kinetic model (PDF)

■ AUTHOR INFORMATION

Corresponding Author

Hao Shen − *Department of Chemistry and Biochemistry, Kent State University, Kent, Ohio 44242, United States;* orcid.org/0000-0002-2798-5861; Email: hshen7@kent.edu

Authors

Li Zuo − *Department of Chemistry and Biochemistry, Kent State University, Kent, Ohio 44242, United States; School of Chemistry and Chemical Engineering, Nanjing University, Nanjing, Jiangsu 210008, China*

Hallie King − *Department of Chemistry and Biochemistry, Kent State University, Kent, Ohio 44242, United States*

Mohammad Akter Hossain − *Department of Chemistry and Biochemistry, Kent State University, Kent, Ohio 44242, United States*

Fatiha Farhana − *Department of Chemistry and Biochemistry, Kent State University, Kent, Ohio 44242, United States*

Madelyn M. Kist − *Department of Chemistry and Biochemistry, Kent State University, Kent, Ohio 44242, United States;* orcid.org/0000-0001-9432-7319

Rebecca L. Stratton − *Department of Chemistry and Biochemistry, Kent State University, Kent, Ohio 44242, United States;* orcid.org/0009-0001-8005-7327

Jiao Chen − *Department of Chemistry and Biochemistry, Kent State University, Kent, Ohio 44242, United States*

Complete contact information is available at: https://pubs.acs.org/10.1021/cbmi.3c00096

Notes

The authors declare no competing financial interest.

■ ACKNOWLEDGMENTS

The authors thank the Farris Family Innovation Award of Kent State University for financial support. H.S. acknowledges the National Science Foundation (NSF) (No. CHE2247709) for grant support.

■ REFERENCES

(1) Liang, M.; Yan, X. Nanozymes: From New Concepts, Mechanisms, and Standards to Applications. *Acc. Chem. Res.* **2019**, *52* (8), 2190−2200.

(2) Wang, H.; Wan, K.; Shi, X. Recent Advances in Nanozyme Research. *Adv. Mater.* **2019**, *31* (45), 1805368.

(3) Wei, H.; Wang, E. Nanomaterials with enzyme-like characteristics (nanozymes): next-generation artificial enzymes. *Chem. Soc. Rev.* **2013**, *42* (14), 6060−6093.

(4) Wu, J.; Wang, X.; Wang, Q.; Lou, Z.; Li, S.; Zhu, Y.; Qin, L.; Wei, H. Nanomaterials with enzyme-like characteristics (nanozymes): next-generation artificial enzymes (II). *Chem. Soc. Rev.* **2019**, *48* (4), 1004−1076.

(5) Chen, L.-L.; Wang, Z.-G.; Zhang, H.; Chen, L.-M.; Zhao, L.; Liu, Z.-Y.; Zhao, W.; Jiang, L.-H.; Ma, A.-X.; Yang, X.; Liu, S.-L.; Zhang, S.; Pang, D.-W. Monitoring Neovascularization of Malignant Solid Tumors with Horseradish Peroxidase-Functionalized Near-Infrared-II PbS Quantum Dots. *Chemical & Biomedical Imaging* **2023**, *1* (1), 81−90.
(6) Lake, R. J.; Yang, Z.; Zhang, J.; Lu, Y. DNAzymes as Activity-Based Sensors for Metal Ions: Recent Applications, Demonstrated Advantages, Current Challenges, and Future Directions. *Acc. Chem. Res.* **2019**, *52* (12), 3275−3286.
(7) Wang, Y.; Nguyen, K.; Spitale, R. C.; Chaput, J. C. A biologically stable DNAzyme that efficiently silences gene expression in cells. *Nat. Chem.* **2021**, *13* (4), 319−326.
(8) Chen, Y.; Wang, P.; Hao, H.; Hong, J.; Li, H.; Ji, S.; Li, A.; Gao, R.; Dong, J.; Han, X.; Liang, M.; Wang, D.; Li, Y. Thermal Atomization of Platinum Nanoparticles into Single Atoms: An Effective Strategy for Engineering High-Performance Nanozymes. *J. Am. Chem. Soc.* **2021**, *143* (44), 18643−18651.
(9) Hu, W. C.; Younis, M. R.; Zhou, Y.; Wang, C.; Xia, X. H. In Situ Fabrication of Ultrasmall Gold Nanoparticles/2D MOFs Hybrid as Nanozyme for Antibacterial Therapy. *Small* **2020**, *16* (23), 2000553.
(10) Hu, Y.; Cheng, H.; Zhao, X.; Wu, J.; Muhammad, F.; Lin, S.; He, J.; Zhou, L.; Zhang, C.; Deng, Y.; Wang, P.; Zhou, Z.; Nie, S.; Wei, H. Surface-Enhanced Raman Scattering Active Gold Nanoparticles with Enzyme-Mimicking Activities for Measuring Glucose and Lactate in Living Tissues. *ACS Nano* **2017**, *11* (6), 5558−5566.
(11) Li, S.; Zhang, Y.; Wang, Q.; Lin, A.; Wei, H. Nanozyme-Enabled Analytical Chemistry. *Anal. Chem.* **2022**, *94* (1), 312−323.
(12) Li, W.; Chen, B.; Zhang, H.; Sun, Y.; Wang, J.; Zhang, J.; Fu, Y. BSA-stabilized Pt nanozyme for peroxidase mimetics and its application on colorimetric detection of mercury(II) ions. *Biosens Bioelectron* **2015**, *66*, 251−258.
(13) Liu, C.; Xing, J.; Akakuru, O. U.; Luo, L.; Sun, S.; Zou, R.; Yu, Z.; Fang, Q.; Wu, A. Nanozymes-Engineered Metal-Organic Frameworks for Catalytic Cascades-Enhanced Synergistic Cancer Therapy. *Nano Lett.* **2019**, *19* (8), 5674−5682.
(14) Zhang, Y.; Wang, F.; Liu, C.; Wang, Z.; Kang, L.; Huang, Y.; Dong, K.; Ren, J.; Qu, X. Nanozyme Decorated Metal-Organic Frameworks for Enhanced Photodynamic Therapy. *ACS Nano* **2018**, *12* (1), 651−661.
(15) Bian, Z.; Tachikawa, T.; Zhang, P.; Fujitsuka, M.; Majima, T. Au/TiO_2 superstructure-based plasmonic photocatalysts exhibiting efficient charge separation and unprecedented activity. *J. Am. Chem. Soc.* **2014**, *136* (1), 458−465.
(16) Yang, S.; Wang, Y.; Wang, Q.; Li, F.; Ling, D. DNA-Driven Dynamic Assembly/Disassembly of Inorganic Nanocrystals for Biomedical Imaging. *Chemical & Biomedical Imaging* **2023**, *1* (4), 340−355.
(17) Cai, C.; Liu, Y.; Zhang, Z.; Tian, T.; Wang, Y.; Wang, L.; Zhang, K.; Liu, B. Activity-Based Self-Enriched SERS Sensor for Blood Metabolite Monitoring. *ACS Appl. Mater. Interfaces* **2023**, *15* (4), 4895−4902.
(18) Huang, Y. F.; Zhang, M.; Zhao, L. B.; Feng, J. M.; Wu, D. Y.; Ren, B.; Tian, Z. Q. Activation of oxygen on gold and silver nanoparticles assisted by surface plasmon resonances. *Angew. Chem. Int. Ed* **2014**, *53* (9), 2353−2357.
(19) Li, J.; Cushing, S. K.; Zheng, P.; Meng, F.; Chu, D.; Wu, N. Plasmon-induced photonic and energy-transfer enhancement of solar water splitting by a hematite nanorod array. *Nat. Commun.* **2013**, *4*, 2651.
(20) Li, J.; Cushing, S. K.; Zheng, P.; Senty, T.; Meng, F.; Bristow, A. D.; Manivannan, A.; Wu, N. Solar hydrogen generation by a CdS-Au-TiO_2 sandwich nanorod array enhanced with Au nanoparticle as electron relay and plasmonic photosensitizer. *J. Am. Chem. Soc.* **2014**, *136* (23), 8438−8449.
(21) Wang, S.; Gao, Y.; Miao, S.; Liu, T.; Mu, L.; Li, R.; Fan, F.; Li, C. Positioning the Water Oxidation Reaction Sites in Plasmonic Photocatalysts. *J. Am. Chem. Soc.* **2017**, *139* (34), 11771−11778.
(22) Zhang, Z.; Zhang, L.; Hedhili, M. N.; Zhang, H.; Wang, P. Plasmonic gold nanocrystals coupled with photonic crystal seamlessly on TiO_2 nanotube photoelectrodes for efficient visible light photoelectrochemical water splitting. *Nano Lett.* **2013**, *13* (1), 14−20.
(23) Li, W.; Miao, J.; Peng, T.; Lv, H.; Wang, J. G.; Li, K.; Zhu, Y.; Li, D. Single-Molecular Catalysis Identifying Activation Energy of the Intermediate Product and Rate-Limiting Step in Plasmonic Photocatalysis. *Nano Lett.* **2020**, *20* (4), 2507−2513.
(24) Zhang, K.; Liu, Y.; Zhao, J.; Liu, B. Nanoscale tracking plasmon-driven photocatalysis in individual nanojunctions by vibrational spectroscopy. *Nanoscale* **2018**, *10* (46), 21742−21747.
(25) Zou, N.; Chen, G.; Mao, X.; Shen, H.; Choudhary, E.; Zhou, X.; Chen, P. Imaging Catalytic Hotspots on Single Plasmonic Nanostructures via Correlated Super-Resolution and Electron Microscopy. *ACS Nano* **2018**, *12* (6), 5570−5579.
(26) Jang, Y. H.; Jang, Y. J.; Kim, S.; Quan, L. N.; Chung, K.; Kim, D. H. Plasmonic Solar Cells: From Rational Design to Mechanism Overview. *Chem. Rev.* **2016**, *116* (24), 14982−15034.
(27) Lu, L.; Luo, Z.; Xu, T.; Yu, L. Cooperative plasmonic effect of Ag and Au nanoparticles on enhancing performance of polymer solar cells. *Nano Lett.* **2013**, *13* (1), 59−64.
(28) Fang, M.; Tan, X.; Liu, Z.; Hu, B.; Wang, X. Recent Progress on Metal-Enhanced Photocatalysis: A Review on the Mechanism. *Research* **2021**, *2021*, 9794329.
(29) Li, S.; Miao, P.; Zhang, Y.; Wu, J.; Zhang, B.; Du, Y.; Han, X.; Sun, J.; Xu, P. Recent Advances in Plasmonic Nanostructures for Enhanced Photocatalysis and Electrocatalysis. *Adv. Mater.* **2021**, *33* (6), 2000086.
(30) Zhang, X.; Chen, Y. L.; Liu, R. S.; Tsai, D. P. Plasmonic photocatalysis. *Rep. Prog. Phys.* **2013**, *76* (4), No. 046401.
(31) Cao, M.; Chang, Z.; Tan, J.; Wang, X.; Zhang, P.; Lin, S.; Liu, J.; Li, A. Superoxide Radical-Mediated Self-Synthesized Au/MoO(3-x) Hybrids with Enhanced Peroxidase-like Activity and Photothermal Effect for Anti-MRSA Therapy. *ACS Appl. Mater. Interfaces* **2022**, *14* (11), 13025−13037.
(32) Feng, J.; Liu, J.; Cheng, X.; Liu, J.; Xu, M.; Zhang, J. Hydrothermal Cation Exchange Enabled Gradual Evolution of Au@ZnS-AgAuS Yolk-Shell Nanocrystals and Their Visible Light Photocatalytic Applications. *Adv. Sci.* **2018**, *5* (1), 1700376.
(33) Huang, X.; Zeng, Z.; Bao, S.; Wang, M.; Qi, X.; Fan, Z.; Zhang, H. Solution-phase epitaxial growth of noble metal nanostructures on dispersible single-layer molybdenum disulfide nanosheets. *Nat. Commun.* **2013**, *4*, 1444.
(34) Aslam, U.; Chavez, S.; Linic, S. Controlling energy flow in multimetallic nanostructures for plasmonic catalysis. *Nat. Nanotechnol* **2017**, *12* (10), 1000−1005.
(35) Wang, C.; Zhao, Y.; Xu, H.; Li, Y.; Wei, Y.; Liu, J.; Zhao, Z. Efficient Z-scheme photocatalysts of ultrathin g-C_3N_4-wrapped Au/TiO_2-nanocrystals for enhanced visible-light-driven conversion of CO_2 with H_2O. *Appl. Catal., B* **2020**, *263*, 118314.
(36) Wu, B.; Liu, D.; Mubeen, S.; Chuong, T. T.; Moskovits, M.; Stucky, G. D. Anisotropic Growth of TiO_2 onto Gold Nanorods for Plasmon-Enhanced Hydrogen Production from Water Reduction. *J. Am. Chem. Soc.* **2016**, *138* (4), 1114−1117.
(37) Bai, S.; Wang, L.; Li, Z.; Xiong, Y. Facet-Engineered Surface and Interface Design of Photocatalytic Materials. *Adv. Sci.* **2017**, *4* (1), 1600216.
(38) Gao, C.; Lyu, F.; Yin, Y. Encapsulated Metal Nanoparticles for Catalysis. *Chem. Rev.* **2021**, *121* (2), 834−881.
(39) Heinz, H.; Pramanik, C.; Heinz, O.; Ding, Y.; Mishra, R. K.; Marchon, D.; Flatt, R. J.; Estrela-Lopis, I.; Llop, J.; Moya, S.; Ziolo, R. F. Nanoparticle decoration with surfactants: Molecular interactions, assembly, and applications. *Surf. Sci. Rep* **2017**, *72* (1), 1−58.
(40) Liu, B.; Liu, J. Surface modification of nanozymes. *Nano Res.* **2017**, *10* (4), 1125−1148.
(41) Ovesny, M.; Krizek, P.; Borkovec, J.; Svindrych, Z.; Hagen, G. M. ThunderSTORM: a comprehensive ImageJ. plug-in for PALM and STORM data analysis and super-resolution imaging. *Bioinformatics* **2014**, *30* (16), 2389−2390.

https://doi.org/10.1021/cbmi.3c00096
Chem. Biomed. Imaging 2023, 1, 760−766

(42) Huang, B.; Wang, W.; Bates, M.; Zhuang, X. Three-Dimensional Super-Resolution Imaging by Stochastic Optical Reconstruction Microscopy. *Science* **2008**, *319* (5864), 810−813.
(43) Zuo, L.; Ren, K.; Guo, X.; Pokhrel, P.; Pokhrel, B.; Hossain, M. A.; Chen, Z. X.; Mao, H.; Shen, H. Amalgamation of DNAzymes and Nanozymes in a Coronazyme. *J. Am. Chem. Soc.* **2023**, *145* (10), 5750−5758.
(44) Jang, D.; Yu, S.; Chung, K.; Yoo, J.; Mota, F. M.; Wang, J.; Ahn, D. J.; Kim, S.; Kim, D. H. Direct deposition of anatase TiO_2 on thermally unstable gold nanobipyramid: Morphology-conserved plasmonic nanohybrid for combinational photothermal and photocatalytic cancer therapy. *Appl. Mater. Today* **2022**, *27*, 101472.
(45) Seh, Z. W.; Liu, S.; Low, M.; Zhang, S. Y.; Liu, Z.; Mlayah, A.; Han, M. Y. Janus Au-TiO_2 photocatalysts with strong localization of plasmonic near-fields for efficient visible-light hydrogen generation. *Adv. Mater.* **2012**, *24* (17), 2310−2314.
(46) Ortega-Liebana, M. C.; Hueso, J. L.; Arenal, R.; Santamaria, J. Titania-coated gold nanorods with expanded photocatalytic response. Enzyme-like glucose oxidation under near-infrared illumination. *Nanoscale* **2017**, *9* (5), 1787−1792.
(47) Li, J.; Liu, W.; Wu, X.; Gao, X. Mechanism of pH-switchable peroxidase and catalase-like activities of gold, silver, platinum and palladium. *Biomaterials* **2015**, *48*, 37−44.
(48) Loynachan, C. N.; Soleimany, A. P.; Dudani, J. S.; Lin, Y.; Najer, A.; Bekdemir, A.; Chen, Q.; Bhatia, S. N.; Stevens, M. M. Renal clearable catalytic gold nanoclusters for in vivo disease monitoring. *Nat. Nanotechnol* **2019**, *14* (9), 883−890.
(49) Tao, Y.; Ju, E.; Ren, J.; Qu, X. Bifunctionalized mesoporous silica-supported gold nanoparticles: intrinsic oxidase and peroxidase catalytic activities for antibacterial applications. *Adv. Mater.* **2015**, *27* (6), 1097−1104.
(50) Yu, Q.; Zhou, J.; Wang, H.; Liu, Y.; Zhou, H.; Kang, B.; Chen, H.-Y.; Xu, J.-J. A Multiple-Response Cascade Nanoreactor for Starvation and Deep Catalysis Chemodynamic Assisted Near-Infrared-II Mild Photothermal Therapy. *Chemical & Biomedical Imaging* **2023**, *1* (3), 242−250.
(51) Shen, H.; Zhou, X.; Zou, N.; Chen, P. Single-Molecule Kinetics Reveals a Hidden Surface Reaction Intermediate in Single-Nanoparticle Catalysis. *J. Phys. Chem. C* **2014**, *118* (46), 26902−26911.
(52) Zhou, X.; Andoy, N. M.; Liu, G.; Choudhary, E.; Han, K. S.; Shen, H.; Chen, P. Quantitative super-resolution imaging uncovers reactivity patterns on single nanocatalysts. *Nat. Nanotechnol* **2012**, *7* (4), 237−241.
(53) Chen, P.; Xu, W.; Zhou, X.; Panda, D.; Kalininskiy, A. Single-nanoparticle catalysis at single-turnover resolution. *Chem. Phys. Lett.* **2009**, *470* (4−6), 151−157.
(54) Xu, W.; Kong, J. S.; Yeh, Y. T.; Chen, P. Single-molecule nanocatalysis reveals heterogeneous reaction pathways and catalytic dynamics. *Nat. Mater.* **2008**, *7* (12), 992−996.
(55) Xu, W.; Kong, J. S.; Chen, P. Single-Molecule Kinetic Theory of Heterogeneous and Enzyme Catalysis. *J. Phys. Chem. C* **2009**, *113* (6), 2393−2404.
(56) Bollhorst, T.; Rezwan, K.; Maas, M. Colloidal capsules: nano- and microcapsules with colloidal particle shells. *Chem. Soc. Rev.* **2017**, *46* (8), 2091−2126.
(57) Gao, Y.; Liu, X.; Sun, L.; Xu, Y.; Yang, S.; Fan, C.; Li, D. Alleviated Inhibition of Single Enzyme in Confined and Crowded Environment. *J. Phys. Chem. Lett.* **2019**, *10* (1), 82−89.
(58) Liu, Y.; Zhang, K.; Tian, X.; Zhou, L.; Liu, J.; Liu, B. Quantitative Single-Particle Fluorescence Imaging Elucidates Semiconductor Shell Influence on Ag@TiO(2) Photocatalysis. *ACS Appl. Mater. Interfaces* **2021**, *13* (6), 7680−7687.
(59) Kang, J.; Park, S. J.; Kim, J. H.; Chen, P.; Sung, J. Stochastic Kinetics of Nanocatalytic Systems. *Phys. Rev. Lett.* **2021**, *126* (12), No. 126001.
(60) Mukherjee, S.; Libisch, F.; Large, N.; Neumann, O.; Brown, L. V.; Cheng, J.; Lassiter, J. B.; Carter, E. A.; Nordlander, P.; Halas, N. J. Hot electrons do the impossible: plasmon-induced dissociation of H_2 on Au. *Nano Lett.* **2013**, *13* (1), 240−247.
(61) Mukherjee, S.; Zhou, L.; Goodman, A. M.; Large, N.; Ayala-Orozco, C.; Zhang, Y.; Nordlander, P.; Halas, N. J. Hot-electron-induced dissociation of H_2 on gold nanoparticles supported on SiO_2. *J. Am. Chem. Soc.* **2014**, *136* (1), 64−67.
(62) Han, K. S.; Liu, G.; Zhou, X.; Medina, R. E.; Chen, P. How does a single Pt nanocatalyst behave in two different reactions? *A single-molecule study. Nano Lett.* **2012**, *12* (3), 1253−1259.

https://doi.org/10.1021/cbmi.3c00096
Chem. Biomed. Imaging 2023, 1, 760−766